Probing Molecular Conformations with Electron Momentum Spectroscopy: The Case of *n*-Butane

M. S. Deleuze,*,† W. N. Pang,‡,§ A. Salam,† and R. C. Shang‡

Contribution from the Departement SBG, Limburgs Universitair Centrum, Universitaire Campus, B3590 Diepenbeek, Belgium, and Polarization Physics Laboratory, Department of Physics, Tsinghua University, Beijing, 100084, China

Received November 16, 2000

Abstract: High-resolution (e,2e) measurements of the valence electronic structure and momentum-space electron density distributions of *n*-butane have been exhaustively reanalyzed in order to cope with the presence of two stable structures in the gas phase, namely the *all-staggered* and *gauche* conformers. The measurements are compared to a series of Boltzmann-weighted simulations based on the momentum-space form of Kohn−Sham (B3LYP) orbital densities, and to ionization spectra obtained from high-level [ADC(3)] one-particle Green's Function calculations. Indubitable improvements in the quality of the simulated (e,2e) ionization spectra and electron momentum profiles are seen when the contributions of the *gauche* form of *n*-butane are included. Both the one-electron binding energies and momentum distributions consistently image the distortions and topological changes that molecular orbitals undergo due to torsion of the carbon backbone, and thereby exhibit variations which can be traced experimentally. With regard to the intimate relation of (e,2e) cross sections with orbital densities, electron momentum spectroscopy can therefore be viewed as a very powerful, but up to now largely unexploited, conformational probe. The study also emphasizes the influence of thermal agitation in photoionization experiments of all kind.

I. Introduction

n-Butane, the prototype of hydrocarbon backbone torsional potentials,[1] represents one of the cornerstones of molecular thermostatistics and conformational analysis.[2] As is well-known, its potential energy surface displays four nonequivalent torsional stationary points with respect to the central carbon−carbon bond. Among these are two energy minima with C_{2h} and C_2 symmetry, the *anti* (or *all-staggered*) and *gauche* conformations, respectively. The less stable conformer, *gauche*, is only about 0.8 kcal mol^{-1} higher in energy than the *anti* conformer. The unique *anti* and the two mirror-image *gauche* energy minima are separated by two nonequivalent saddle points, of which the lowest requires approximately 3.2 kcal mol^{-1} activation energy for the conversion of the *anti* into one of the two *gauche* conformers, whereas the highest, which lies at about 5 kcal mol^{-1} above the global energy minimum, corresponds to the unique *cis* (or *syn*) transition state between the two *gauche* minima.

Since the pioneering work[3] by Pitzer in 1940, the *anti*/*gauche* enthalpy differences in gas, liquid and solution phases or the relative conformer abundances at various temperatures have been investigated extensively by means of thermostatistics,[4] Raman,[5] far-infrared,[6] and NMR[7] spectroscopy, ultrasonic relaxation,[8] electron diffraction,[9] and quite naturally quantum mechanics[10] (for a compilation of the earliest results, see also refs 11). The

* Corresponding author. E-mail: deleuze@luc.ac.be.
† Limburgs Universitair Centrum.
‡ Tsinghua University.
§ Present address: Dr. Wenning Pang, Physikalisches Institut, Universität Münster, D48149 Münster, Germany.

(1) (a) Bartell, L. S.; Kohl, D. A. *J. Chem. Phys.* **1963**, *39*, 1963. (b) Goodman, J. M. *J. Chem. Inf. Comput. Sci.* **1997**, *37*, 876. (c) Gotô, H.; Ôsawa, E.; Yamato, M. *Tetrahedron* **1993**, *49*, 387. (d) Tasi, G.; Mizukamim, F.; Palinko, I.; Csontos, J.; Gyorffy, W.; Nair, P.; Maeda, K.; Toba, M.; Niwa, S.; Kioyozumi, Y.; Kiricsi, I. *J. Phys. Chem. A* **1998**, *102*, 7698.

(2) (a) Eliel, E. L.; Allinger, N. L.; Angyal, S. J.; Morrison, G. A. *Conformational Analysis*; Wiley: New York, 1965. (b) Burkert, U.; Allinger, N. L. *Molecular Mechanics*; American Chemical Society: Washington DC, 1982. (c) Lipton, M.; Still, W. C. *J. Comput. Chem.* **1988**, *9*, 343. (d) Nair, N.; Goodman, J. M. *J. Chem. Inf. Comput. Sci.* **1998**, *39*, 317. (e) Fraser, G. T.; Suenram, R. D.; Lugez, C. L. *J. Phys. Chem. A.* **2000**, *104*, 1141.

(3) Pitzer, K. S. *J. Chem. Phys.* **1940**, *8*, 711.

(4) Ito, K. *J. Am. Chem. Soc.* **1953**, *75*, 2430.

(5) (a) Sheppard, N.; Szasz, G. J.; Rank, D. H. *J. Chem. Phys.* **1948**, *16*, 704. (b) Sheppard, N.; Szasz, G. J. *J. Chem. Phys.* **1949**, *17*, 86. (c) Verma, A. L.; Murphy, W. F.; Bernstein, H. J. *J. Chem. Phys.* **1974**, *60*, 1540. (d) Devaure, J.; Lascombe, J. *Nouv. J. Chim.* **1979**, *3*, 579. (e) Kint, S.; Scherer, J. R.; Snyder, R. G. *J. Chem. Phys.* **1980**, *73*, 2599. (f) Rosenthal, L.; Rabolt, J. F.; Hummel, J. *J. Chem. Phys.* **1982**, *76*, 817. (g) Murphy, W. F.; Ferandez-Sanchez, J. M.; Raghavachari, K. *J. Phys. Chem.* **1991**, *95*, 1124, (h) Murphy, W. F. *J. Raman Spectrosc.* **1992**, *23*, 413.

(6) (a) Durig, J. R.; Compton, D. A. *J. Phys. Chem.* **1979**, *83*, 265. (b) Stidham, H. D.; Durig, J. R. *Spectrochim. Acta, Part A* **1986** *42*, 105. (c) Durig, J. R.; Wang, A.; Beshir, W.; Little, T. S. *J. Raman Spectrosc.* **1991**, *22*, 683. (d) Herrebout, W. A.; van der Veken, B. J.; Wang, A.; Durig, J. R. *J. Phys. Chem.* **1995**, *99*, 578.

(7) Woller, P. B.; Garbisch, E. W., Jr. *J. Am. Chem. Soc.* **1972**, *94*, 5310.

(8) Piercy, J. E.; Rao, M. G. S. *J. Chem. Phys.* **1967**, *46*, 3951.

(9) (a) Bonham, R. A.; Bartell, L. S. *J. Am. Chem. Soc.* **1959**, *81*, 3951. (b) Bartell, L. S.; Kohl, D. A. *J. Chem. Phys.* **1963**, *39*, 3097. (c) Bradford, W. F.; Fitzwater, S.; Bartell, L. S. *J. Mol. Struct.* **1977**, *38*, 185. (d) Heenan, R. K.; Bartell, L. S. *J. Chem. Phys.* **1983**, *78*, 1270.

(10) (a) Hoylan, J. R. *J. Chem. Phys.* **1968**, *49*, 2563. (b) Radom, L.; Lathan, W. A.; Hehre, W. J.; Pople, J. A. *J. Am. Chem. Soc.* **1973**, *95*, 693. (c) Peterson, M. R.; Csizmadia, I. G. *J. Am. Chem. Soc.* **1978**, *100*, 6911. (d) Allinger, N. L.; Profeta, S., Jr. *J. Comput. Chem.* **1980**, *1*, 181. (e) Darsey, J. A.; Rao, B. K. *Macromolecules* **1981**, *14*, 1575. (f) Van-Catledge, F. A.; Allinger, N. L. *J. Am. Chem. Soc.* **1982**, *104*, 6272. (g) Raghavachari, K. *J. Chem. Phys.* **1984**, *81*, 1383. (h) Steele, D. *J. Chem. Soc., Faraday Trans. 2* **1985**, *81*, 1077. (i) Wiberg, K. B.; Murcko, M. A. *J. Am. Chem. Soc.* **1988**, *110*, 8029. (j) Allinger, N. L.; Grev, R. S.; Yates, B. F.; Schaefer, H. F., III. *J. Am. Chem. Soc.* **1990**, *112*, 114. (k) Murcko, M. A.; Castejon, H.; Wiberg, K. B. *J. Phys. Chem.* **1996**, *100*, 16162. (l) Smith, G. D.; Jaffe, R. L. *J. Phys. Chem.* **1996**, *100*, 18718.

(11) (a) Chen, S. S.; Wilhoit, R. C.; Zwolinski, B. J. *J. Phys. Chem. Ref. Data* **1975**, *4*, 859. (b) Compton, D. A. C.; Montero, S.; Murphy, W. F. *J. Phys. Chem.* **1980**, 84, 3587.

10.1021/ja0039886 CCC: $20.00
Published on Web 04/05/2001

most systematic and involved *ab initio* theoretical study[12] reported so far is based on a focal point extrapolation to the Schrödinger limit in the Born−Oppenheimer approximation of the conformational energy barriers using increasingly complete basis sets (up to 840 functions) and treatments of electron correlation [up to the CCSD(T) level of theory]. With regard to internal energies, this study places the *gauche* form 0.62 kcal mol^{-1} above the *anti* conformer, in excellent agreement with the latest revision (0.67 ± 0.10 kcal mol^{-1}) in the spectroscopic work of Durig and co-workers.[6d]

Compared with the many investigations of the molecular structure of *n*-butane, detailed studies of the electronic structure of this, at first glance not very challenging, compound are relatively scarce. Early works on the ionization properties of *n*-butane comprise the X-ray photoemission spectroscopy (XPS) study by Pireaux et al.,[13] the HeI ultraviolet photoemission spectroscopy (UPS) by Kimura et al.,[14] as well as the more extended HeII UPS measurements of Price[15] et al., and Potts and Streets.[16] These works have mainly highlighted the traditional aspects of high-resolution photoelectron spectroscopy, that is, they have focused on the correct assignment of most ionization levels, under the assumption of a one-to-one correspondence between the recorded lines and the valence one-electron (i.e., orbital) energy levels of the *most stable* conformation. Their outcome must be evaluated within the framework of polymer and material sciences, in particular for their invaluable contribution to the understanding of the construction principles of the electronic band structure of polyethylene[17] and related large paraffine chains such as hexatriacontane ($C_{36}H_{74}$).[18] Prior to direct angular-resolved measurements,[19] this band structure was first extrapolated from a systematic study of the X-ray photoionization spectra of the shortest terms of the *n*-alkane series,[13,20] from methane up to tridecane ($C_{13}H_{28}$).

More recently, following the identification and analysis of striking spectral signatures for alterations of the molecular conformation of *n*-alkane or cycloalkane compounds,[21] photoelectron measurements on saturated hydrocarbons have been systematically reinvestigated beyond the one-electron or quasi-particle picture on the basis of advanced Green's Function calculations, [22] in order to cope consistently with initial and final state configuration interactions. In the case of *n*-butane, the latter gave evidence for a severe breakdown of the orbital picture of ionization for the innermost $3a_g$ one-electron level,[22a] which in the spectrum appears as a broad set of shake-up lines centered at about 25 eV, accompanied by a correlation tail extending up to at least 60 eV.[22b] Preliminary electron momentum spectroscopy measurements[23] (EMS, also referred to as binary (e,2e) spectroscopy[24]) have confirmed the quasi-exclusive relationship of the spectral features recorded at electron binding energies of ~24 eV and beyond. These measurements have in turn been analyzed in detail[25] on the sole *all-staggered* form of *n*-butane using high-order Green's Function ionization energies and Kohn−Sham Density Functional orbitals derived from large basis set calculations.

Ample studies have demonstrated the efficiency of EMS as a particularly sensitive orbital imaging technique, capable of providing detailed information both on electron binding energies throughout the whole valence region, and on the orbital electron density distributions.[26−30] At high electron impact energy, according to the plane wave impulse and the sudden (i.e., target Hartree−Fock [HF] or target Kohn−Sham [KS]) approximations,[23] the one-electron EMS cross sections (i.e., momentum distributions) are given by

$$\sigma = \text{constant} \int d\Omega |\psi_i(\boldsymbol{p})|^2 \qquad (1)$$

where $\boldsymbol{p}$ can be equated to the momentum of the ionized electron *prior* to the ionization of the molecular target, and the momentum-space one-electron wave function $\psi_i(\boldsymbol{p})$ is the

(12) Allinger, N. L.; Fermann, J. T.; Allen, W. D.; Schaefer, H. F., III. *J. Chem. Phys.* **1997**, *106*, 5143.

(13) Pireaux, J.-J.; Svensson, S.; Basilier, E.; Malmqvist, P.-A.; Gelius, U.; Caudano, R.; Siegbahn, K. *Phys. Rev. A.* **1976**, *14*, 2133.

(14) Kimura, K.; Katsumata, S.; Achiba, Y.; Yamazaki, T.; Iwata, S. *Handbook of HeI Photoelectron Spectra of Fundamental Organic Molecules*; Japan Scientific Society: Tokyo, 1981.

(15) Price, W. C.; Potts, A. W.; Streets, D. G. In *Electron Spectroscopy*: Shirley, D. A., Ed.; North: Holland, Amsterdam, 1972; p 187.

(16) Potts, A. W.; Streets, D. *J. Chem. Soc., Faraday Trans. II* **1974**, *2*, 875.

(17) For a review, see, e.g.: Karpfen., A. *J. Chem. Phys.* **1981**, *75*, 238.

(18) (a) Delhalle, J.; André, J.-M.; Delhalle, S.; Pireaux, J. J.; Caudano, R.; Verbist, J. J. *J. Chem. Phys.* **1974**, *60*, 595.

(19) (a) Seki, K.; Karlsson, U.; Engelhardt, R.; Koch, E. E. *Chem. Phys. Lett.* **1984**, *103*, 343. (b) Seki, K.; Ueno, N.; Karlsson, U. O.; Emgelhardt, R.; Koch, E. E. *Chem. Phys.* **1986**, *105*, 247. (c) Fujimoto, H.; Mori, T.; Inokuchi, H.; Ueno, N.; Sugita, K.; Seki, K. *Chem. Phys. Lett.* **1987**, *141*, 485. (d) Ueno, N.; Seki, K.; Sato, N.; Fujimoto, H.; Kuramochi, T.; Sugita, K.; Inokuchi, H. *Phys. Rev. B* **1990**, *41*, 1176.

(20) (a) Pireaux, J.-J.; Svensson, S.; Basilier, E.; Malmqvist, P.-A.; Gelius, U.; Caudano, R.; Siegbahn, K. *J. Phys.* (in French) **1977**, *38*, 1213. (b) Pireaux, J.-J.; Svensson, S.; Basilier, E.; Malmqvist, P.-A.; Gelius, U.; Caudano, R.; Siegbahn, K. *J. Phys.* (in French) **1977**, *38*, 1221. (c) Pireaux, J. J.; Caudano, R. *Phys. Rev. B* **1977**, *15*, 2242. (d) Pireaux, J. J.; Caudano, R. *Am. J. Phys.* **1984**, *52*, 821.

(21) (a) Deleuze, M.; Denis, J.-P.; Delhalle, J.; Pickup, B. T. *J. Phys. Chem.* **1993**, *97*, 5115. (b) Deleuze, M.; Delhalle, J.; Pickup, B. T. *J. Phys. Chem.* **1994**, *98*, 2382. (c) Deleuze, M.; Delhalle, J.; Pickup, B. T.; Svensson, S. *J. Am. Chem. Soc.* **1994**, *116*, 10715. (d) Riga, J.; Delhalle, J.; Deleuze, M.; Pireaux, J. J.; Verbist, J. *Surf. Interface Anal.* **1994**, *22*, 507. (e) Duwez, A. S.; Di Paolo, S.; Ghijsens, J.; Riga, J.; Deleuze, M.; Delhalle, J. *J. Phys. Chem. B* **1997**, *101*, 884.

(22) (a) Deleuze, M.; Cederbaum, L. S. *J. Chem. Phys.* **1996**, *105*, 7583. (b) Golod, A.; Deleuze, M.; Cederbaum, L. S. *J. Chem. Phys.* **1999**, *110*, 6014. (c) Deleuze, M.; Cederbaum, L. S. *Adv. Quantum Chem.* **1999**, *35*, 77.

(23) Pang, W.; Shang, R.; Gao, J.; Gao, N.; Chen, X.; Deleuze, M. *Chem. Phys. Lett.* **1998**, *296*, 605.

(24) (a) McCarthy, I. E.; Weigold, E. *Rep. Prog. Phys.* **1988**, *51*, 299. (b) Leung, K. T. In *Molecular Spectroscopy, Electronic Structure and Intermolecular Interactions*; Maksic, Z. B., Ed.; Springer: Berlin, 1991; p 339. (c) McCarthy, I. E.; Weigold, E. *Rep. Prog. Phys.* **1991**, *54*, 789. (d) Coplan, M. A.; Moore, J. H.; Doering, J. P. *Rev. Modern. Phys.* **1994**, *66*, 985.

(25) Pang, W. N.; Gao, J. F.; Ruan, C. J.; Shang, R. C.; Trofimov, A. B.; Deleuze, M. S. *J. Chem. Phys.* **2000**, *112*, 8043.

(26) (a) Weigold, E. *J. Electron. Spectrosc. Relat. Phenom.* **1990**, *51*, 629. (b) Zheng, Y.; Weigold, W.; Brion, C. E.; von Niessen, W. *J. Electron Spectrosc. Relat. Phenom.* **1990**, *53*, 153. (c) Cook, J. P. D.; Pascual, R.; Weigold, E.; von Niessen, W.; Tomasello, P. *Chem. Phys.* **1990**, *41*, 211. (d) Clark, S. A. C.; Reddish, T. J.; Brion, C. E.; Davidson, E. R.; Frey, R. F. *Chem. Phys.* **1990**, *143*, 1. (e) Weigold, E.; Zheng, Y.; von Niessen, W. *Chem. Phys.* **1991**, *150*, 405.

(27) (a) Hollebone, B. P.; Zheng, Y.; Brion, C. E.; Davidson, E. R.; Feller, D. *Chem. Phys.* **1993**, *171*, 303. (b) Subramaniam, C. K.; Coplan, M. A.; Tossel, J. A.; Moore, J. H.; Leung, K. T. *Chem. Phys.* **1994**, *185*, 237. (c) Samardzic, O.; Weigold, E.; von Niessen, W.; Zakrzewski, V. G.; Brunger, M. J. *Chem. Phys.* **1994**, *182*, 361. (d) Zheng, Y.; Neville, J. J.; Brion, C. E.; Wang, Y.; Davidson, E. R. *Chem. Phys.* **1994**, *188*, 109.

(28) Zheng, Y.; Neville, J. J.; Brion, C. E. *Science* **1995**, *270*, 786.

(29) (a) Hollebone, B. P.; Neville, J. J.; Zheng, Y.; Brion, C. E.; Wang, Y.; Davidson, E. R. *Chem. Phys.* **1995**, *196*, 13. (b) Zheng, Y.; Brion, C. E.; Brunger, M. J.; Zhao, K.; Grisogono, A. M.; Braidwood, S.; Weigold, E.; Chakravorty, S. J.; Davidson, E. R.; Sgamellotti, A.; von Niessen, W. *Chem. Phys.* **1996**, *212*, 269. (c) Neville, J. J.; Zheng, Y.; Brion, C. E. *J. Am. Chem. Soc.* **1996**, *118*, 10533. (d) Neville, J. J.; Zheng, Y.; Hollebone, B. P.; Cann, N. M.; Brion, C. E.; Kim, C. K.; Wolfe, S. *Can J. Phys.* **1996**, *74*, 773.

(30) (a) Rolke, J.; Zheng, Y.; Brion, C. E.; Chakravorty, S. J.; Davidson, E. R.; McCarthy, I. E. *Chem. Phys.* **1997**, *215*, 191. (b) Fan, X. W.; Chen, X. J.; Zhou, S. J.; Zheng, Y.; Brion, C. E.; Frey, R.; Davidson, E. R. *Chem. Phys. Lett.* **1997**, *276*, 346. (c) Rolke, J.; Zheng, Y.; Brion, C. E.; Wang, Y. A.; Davidson, E. R. *Chem. Phys.* **1998**, *230*, 153. (d) Zheng, Y.; Pang, W. N.; Shang, R. C.; Chen, X. J.; Brion, C. E.; Ghanty, T. K.; Davidson, E. R. *J. Chem. Phys.* **1999**, *111*, 9526.

Fourier transform of the more familiar position-space one-electron wave function, most commonly taken as the HF or KS orbital relating to the ionized electron level. Thus, the measured cross sections are spherical averages over the molecular orientations of structure factors, $|\psi_i(\boldsymbol{p})|^2$, derived as momentum-space orbital densities.

From its intimate relationship with molecular orbitals, electron momentum spectroscopy must therefore clearly be one of the best-suited tools for tracing molecular conformations in the gas phase, when the spectrometer resolution permits a sufficiently safe distinction or deconvolution of the ionization lines. The purpose of this work is to demonstrate this capacity and to evaluate the current limits of EMS as a conformational probe, by reconsidering and improving the analysis presented in refs 22 and 25 on the basis of a Boltzmann-weighted average of the ionization spectra and orbital density profiles of the *all-staggered* and *gauche* forms of *n*-butane.

II Computational Details

The calculations presented in this work are based on ground-state geometries of *n*-butane that were optimized for the *all-staggered* and *gauche* forms using Density Functional theory, employing the 6-311++G** basis set[31] and the nonlocal hybrid Becke three-parameter Lee−Yang−Parr functional (B3LYP).[32] The momentum-space orbital densities were obtained by Fourier transform of B3LYP Kohn−Sham (KS) molecular orbitals generated with the GAUSSIAN94 package.[33] This transformation has been carried out by means of the Gaussian weighted planar grid (GW−PG) method of Duffy et al.,[34] in order to deal with the limited resolution (δp), 0.1 atomic units (a.u.), of the (e,2e) spectrometer[25,30d,35] in momentum space. Comparison of the momentum orbital densities with the out-of-plane (or azimuthal) angular dependence of the recorded (e,2e) intensities was achieved for the symmetric noncoplanar kinematics already described in ref 25, considering the same impact and scattering electron energies as those used in the experimental set up, i.e 1200 eV plus ionization energy and 600 eV, respectively. Under these conditions, the electron momentum values (in atomic units, a.u.) that are selected at a given azimuthal angle ϕ are given by:

$$p = \sqrt{(2p_a \cos\theta - p_0)^2 + (2p_a \sin\theta \sin(\phi/2)^2)} \qquad (2)$$

with $\theta = 45°$, $p_a = 6.64077$ a.u. and $p_0 = 0.271105\sqrt{(1200+\mathrm{IP})}$. In this work, the conversion has been achieved using the 1p-GF/ADC(3) results for the ionization energies (IP, in eV).

Vertical ionization spectra are computed by means of the one-particle Green's function (1p-GF)[36] derived from the so-called third-order algebraic-diagrammatic construction scheme [ADC(3)].[37−39] Charge-consistency and thereby the size-intensivity of the ADC(3) results are enforced using the electron density rescaling procedure of ref 40. Briefly, ionized states are described in this scheme in terms of one-hole (1h) and two-hole-one-particle (2h-1p) electronic configurations, which are treated consistently through third- and first-order in the correlation potential, respectively, by virtue of the ADC(3) secular equations. The resulting eigenvalues relate directly to ionization energies, IP_n, while the associated eigenvectors provide Feynman−Dyson transition amplitudes:

$$x_j^n = \langle \psi_n^{N-1} | a_j | \psi_0^N \rangle \qquad (3)$$

These are defined as the couplings between the ionized states ψ_n^{N-1} and the initial ground state ψ_0^N through the interplay of an operator, a_j, describing annihilation of an electron in orbital ψ_j. Since Kohn−Sham orbitals are known[41] to be an excellent approximation to Dyson orbitals,[42] their relationship to (e,2e) line intensities is then straightforward:

$$\sigma_n(\boldsymbol{p}) = \text{constant} \sum_j |x_j^n|^2 |\psi_j(\boldsymbol{p})|^2 \qquad (4)$$

The ADC(3) computations reported in ref 25 for the *all-staggered* form of *n*-butane demonstrate that one-electron ionization energies are practically insensitive to inclusion of diffuse functions in the basis set. In the inner-valence region, improvements of the basis set result in a redistribution of the shake-up intensity, but without any significant influence on the shape and width of the convoluted bands. Diffuse functions have therefore been dropped from the present ADC(3) computations, which because of the lower symmetry of the *gauche* form would else become practically untractable by current computer standards. For the sake of consistency, all the ADC(3) calculations described in this work have therefore been completed with a triple-ζ polarized 6-311G** basis, by means of the original code[43] interfaced to the GAMESS package.[44] The ionization energies have been extracted from the secular ADC(3) matrix using a Block−Davidson diagonalization procedure,[45] with a threshold on pole strengths of 0.005.

Ionization spectra are simulated using as convolution function a Gaussian with a constant FWHM (full width at half the maximum) parameter of 1.7 eV, to approximate the resolution found in the experimental spectra. The (e,2e) spectra and orbital density distributions shown in the sequel are calculated according to a Boltzmann-thermostatistical evaluation of the conformer abundances at room temperature (298 K), in line with the average conditions under which the EMS measurements have been completed.[23,25] The entropies as well as the zero-point vibrational energies (Table 1) used in this evaluation derive from a population analysis within the RRHO (rigid rotors−harmonic oscillators) approximation, on the basis of B3LYP/6-311++G** structures and vibrational frequencies obtained with

Table 1. Thermostatistical Properties of the *all-staggered* and *gauche* Forms of *n*-butane (B3LYP/6-311++G** Results).

	all-staggered form	*gauche* form
ZPE^{vib} (kcal mol $^{-1}$)	82.38741	82.49523
S^{vib} (cal mol^{-1} K^{-1})	10.647	10.350
S^{rot} (cal mol^{-1} K^{-1})	23.156	23.291

(31) (a) Krishnan, R.; Binkley, J. S.; Seeger, R.; Pople, J. A. *J. Chem. Phys.* **1980**, *72*, 650. (b) Clark, T.; Chandrasekhar, J.; Spitznagel, G. W.; Schleyer, P. v. R. *J. Comput. Chem.* **1983**, *4*, 294.

(32) Becke, A. D. *J. Chem. Phys.* **1993**, *98*, 5648. (b) Lee, C.; Yang, W.; Parr, R. G. *Phys. Rev. B* **1988**, *37*, 785.

(33) Frisch, M. J.; Trucks, G. W.; Schlegel, H. B.; Gill, P. M. W.; Johnson, B. G.; Robb, M. A.; Cheeseman, J. R.; Keith, T. A.; Petersson, G. A.; Montgomery, J. A.; Raghavachari, K.; Al-Laham, M. A.; Zakrzewski, V. G.; Ortiz, J. V.; Foresman, J. B.; Cioslowski, J.; Stefanov, B. B.; Nayakkara, A.; Challacombe, M.; Peng, C. Y.; Ayala, P. Y.; Chen, W.; Wong, M. W.; Andres, J. L.; Replogle, E. S.; Gomperts, R.; Martin, R. L.; Fox, D. J.; Binkley, J. S.; Defrees, D. J.; Baker, J.; Stewart, J. P.; Head-Gordon, M.; Gonzales, C.; Pople, J. A. *Gaussian 94*; Gaussian, Inc.: Pittsburgh, PA, 1995.

(34) Duffy, P.; Casida, M. E.; Brion, C. E.; Chong, D. P. *Chem. Phys.* **1992**, *159*, 347.

(35) Chen, X. J. *Aust. J. Phys.* **1998**, *51*, 619.

(36) (a) Cederbaum, L. S.; Domcke, W. *Adv. Chem. Phys.* **1977**, *36*, 205. (b) Öhrn, Y.; Born, G. *Adv. Quantum Chem.* **1981**, *13*, 1. (c) Ortiz, J. V.; in *Computational Chemistry: Reviews of Current trends*; Leszczyinski, J., Ed.; World Scientific: Singapore, 1997; Vol. 2, p 1.

(37) Schirmer, J.; Cederbaum, L. S.; Walter, O. *Phys. Rev. A* **1983**, *28*, 1237.

(38) von Niessen, W.; Schirmer, J.; Cederbaum, L. S. *Comput. Phys. Rep.* **1984**, *1*, 57.

(39) Schirmer, J.; Angonoa, G. *J. Chem. Phys.* **1989**, *91*, 1754.

(40) Deleuze, M.; Scheller, M. K.; Cederbaum, L. S. *J. Chem. Phys.* **1995**, *103*, 3578.

(41) Duffy, P.; Chong, D.; Casida, M. E.; Salahub, D. R. *Phys. Rev. A* **1994**, *50*, 5707.

(42) Deleuze, M.; Pickup, B. T.; Delhalle, J. *Mol. Phys.* **1995**, *83*, 655.

(43) The ADC(3) code developed by Scheller, M. K.; Angonoa, G.; Walter, O.; Schirmer, J. Contributions due to Trofimov, A. B.

(44) Schmidt, M. W.; Baldridge, K. K.; Jensen, J. H.; Koseki, S.; Gordon, M. S.; Nguyen, K. A.; Windus, T. L.; Elbert., S. T.; *QCPE, Bull.* **1990** *10*, 52.

(45) (a) Liu, B. In *Numerical Algorithms in Chemistry, Algebraic Methods*, LBL-8158; Lawrence Berkeley Laboratory, University of California: Springfield, VA, 1978. (b) Tarantelli, F. Unpublished. (c) Tarantelli, F.; Sgamellotti, A.; Cederbaum, L. S.; Schirmer, J.; *J. Chem. Phys.* **1987**, *86*, 2201.

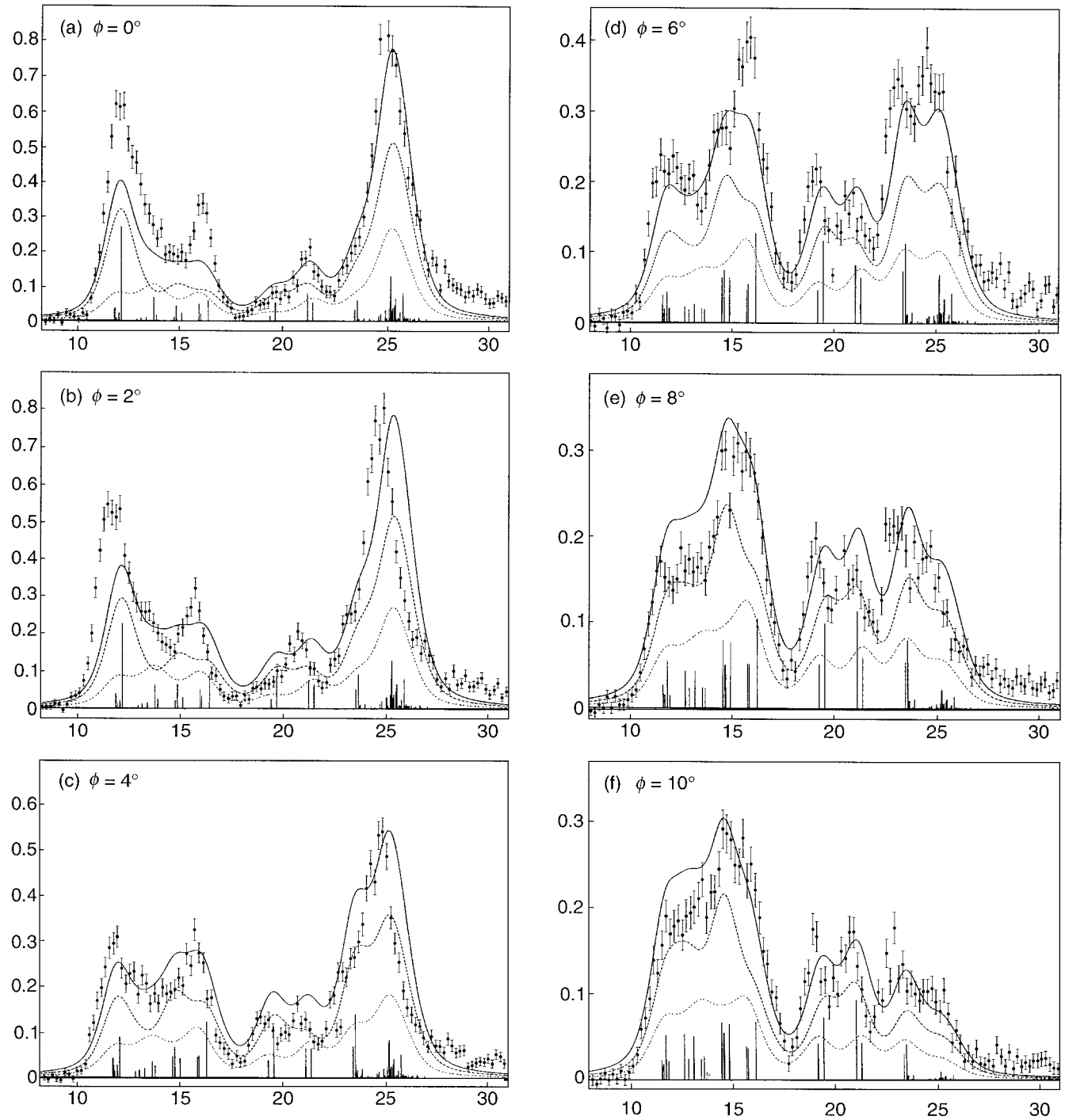

Figure 1. Experimental and theoretical (e,2e) ionization spectra of *n*-butane at different azimuthal angles. Dashed line: Boltzmann weighted contribution (65%) of the *all-staggered* form; dotted line: Boltzmann weighted contribution (35%) of the *gauche* form; full line: total (e,2e) theoretical ionization spectrum. [Relative intensities (in arbitrary units) versus electron binding energies (in eV)].

GAUSSIAN98.[46] From these thermodynamical data and Allinger's best estimate (0.62 kcal mol^{-1}) for the *anti*/*gauche* (internal) energy difference,[12] an *anti* mole fraction of 0.65 is found at room temperature, in fair agreement with the value (0.62 ± 0.04) inferred from the latest spectroscopic work of Durig and co-workers.[6d]

(46) Frisch, M. J.; Trucks, G. W.; Schlegel, H. B.; Scuseria, G. E.; Robb, M. A.; Cheeseman, J. R.; Zakrzewski, V. G.; Montgomery, J. A. Jr.; Stratmann, R. E.; Burant, J. C.; Dapprich, S.; Millam, J. M.; Daniels, A. D.; Kudin, K. N.; Strain, M. C.; Farkas, O.; Tomasi, J.; Barone, V.; Cossi, M.; Cammi, R.; Mennucci, B.; Pomelli, C.; Adamo, C.; Clifford, S.; Ochterski, J.; Petersson, G. A.; Ayala, P. Y.; Cui, Q.; Morokuma, K.; Malick, D. K.; Rabuck, A. D.; Raghavachari, K.; Foresman, J. B.; Cioslowski, J.; Ortiz, J. V.; Baboul, A. G.; Stefanov, B. B.; Liu, G.; Liashenko, A.; Piskorz, P.; Komaromi, I.; Gomperts, R.; Martin, R. L.; Fox, D. J.; Keith, T.; Al-Laham, M. A.; Peng, C. Y.; Nanayakkara, A.; Gonzalez, C.; Challacombe, M.; Gill, P. M. W.; Johnson, B.; Chen, W.; Wong, M. W.; Andres, J. L.; Gonzalez, C.; Head-Gordon, M.; Replogle, E. S.; Pople, J. A. *GAUSSIAN 98*, revision A.6; Gaussian, Inc.: Pittsburgh, PA, 1998.

III. Results and Discussion

III. A. Orbital Energies and Ionization Spectra. The (e,2e) ionization spectra of *n*-butane recorded[25] at out-of-plane scattering angles ϕ of 0, 2, 4, 6, 8, and 10° are displayed in Figure 1a−1f, respectively, together with the simulated EMS profiles for the conformer mixture at room temperature (solid line), as well as with the individual Boltzmann-weighted contributions (dashed and dotted lines). From a comparison of

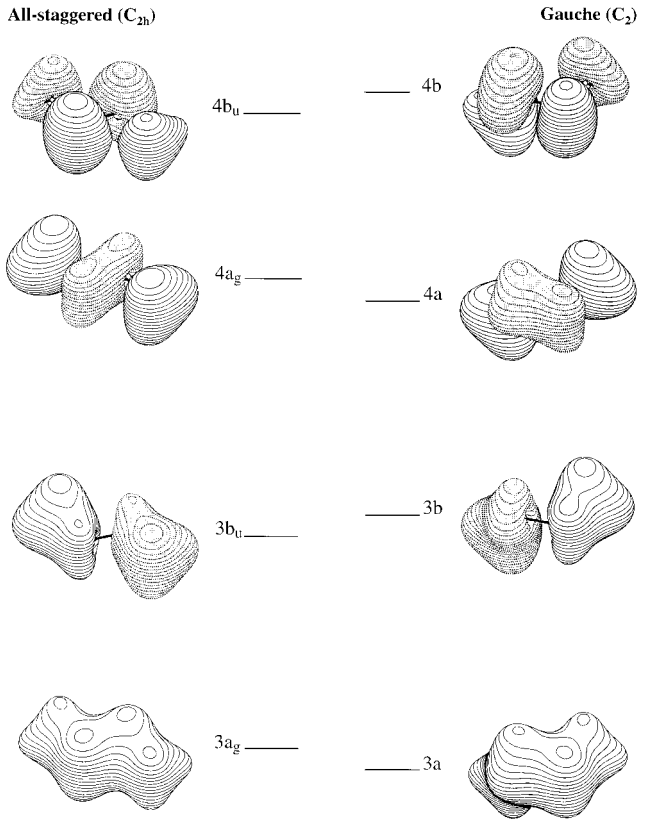

Figure 2. *anti*−*gauche* orbital correlation in the inner-valence region of *n*-butane.

these profiles, it is immediately apparent that changes in the conformation of *n*-butane have a substantial impact on the global appearance of the ionization bands. Significant improvement in the shape and the position of peaks or minima are observed overall for all values of ϕ when consistently accounting for the *gauche* conformer. The improvement is particularly noticeable at ionization energies between 10 and 18 eV and readily confirms the significance of this new investigation, as well as the high quality of the computed (e,2e) cross sections and ionization energies.

The *all-staggered* and *gauche* forms of butane belong to the C_{2h} and C_2 symmetry point groups, respectively. Considering the HF/6-311G** orbital energy order, the *all-staggered* form exhibits in its electronic ground state (X^1A_g) the following inner- and outer valence shell configurations:

$$\{(3a_g)^2(3b_u)^2(4a_g)^2(4b_u)^2\};$$

$$\{(1a_u)^2(5a_g)^2(5b_u)^2(1b_g)^2(6b_u)^2(2a_u)^2(6a_g)^2(2b_g)^2(7a_g)^2\}$$

Similarly, the inner- and outer-valence shell configurations for the *gauche* form of *n*-butane in its electronic ground state (X^1A) are:

$$\{(3a)^2(3b)^2(4a)^2(4b)^2\};$$

$$\{(5b)^2(5a)^2(6a)^2(6b)^2(7a)^2(7b)^2(8a)^2(8b)^2(9a)^2\}$$

The valence orbitals of the two forms of *n*-butane are correlated through the diagrams of Figures 2 and 3, which have been drawn from HF orbital contours and orbital energies (Table 2). From these figures, it appears overall that fully symmetric orbitals are stabilized substantially when *n*-butane evolves from its *all-staggered* into its *gauche* forms. This is due to enhanced through-space bonding interactions between atomic functions centered on terminal methyl groups ($3a_g$, $4a_g$, $6a_g$) or around the central carbon bond ($5a_g$). In contrast, most of the nonfully symmetric levels are destabilized by torsion, due to stronger through-space antibonding interactions between the end groups ($3b_u$, $4b_u$, $1a_u$, $6b_u$) or the disruption of bonding interactions around the central carbon bond ($5b_u$). The energy variations, +0.93 and −1.11 eV, are markedly stronger for the $5a_g$ and $5b_u$ levels, and thereby closely fingerprint the deeper impact of torsion on their orbital topology. The *all-staggered* $5b_u$ and $6b_u$ orbitals correlate with the 6b and 7b orbitals in the *gauche* form, respectively, which implies a reversal of the energy order with the $1b_g$ and $2a_u$ orbitals (alias 6a and 7a).

Although the inclusion of electronic correlation and relaxation effects result in energy shifts by ∼0.8 to ∼2.4 eV on one-electron binding energies, the energy order found at the ADC-(3) level (Table 2) is strictly identical to the HF one. Comparison of the peak positions (Table 2) inferred from the thermally averaged ADC(3) simulations with experimental data of various origins[13−16] indicate errors on one-electron ionization energies ranging from ∼0.5 eV in the inner-valence region down to ∼0.1 eV in the outer-valence region. The interesting case of the HeI measurements by Kimura et al.[14] is discussed in an Appendix to this paper, where it is shown that high-resolution UPS measurements on *n*-butane may also disclose detailed information on the average effect of thermal motions on the molecular structure.

Despite the rather large bandwidth parameter and conformational mixing, four peaks related to ionization of the four inner-valence orbitals $3a_g$ − 3a, $3b_u$ − 3b, $4a_g$ − 4a and $4b_u$ − 4b can be observed at about 25.25, 23.51, 21.14 and 19.40 eV, respectively, in the (e,2e) spectra simulated from the 1p-GF/ADC(3) results for values of ϕ between 4 and 8°. On the experimental side, these four peaks were consistently resolved near 24.7 ± 0.1, 23.0 ±0.1, 20.8 ±0.1 and 19.0 ±0.1 eV (Table 2).

As for the $3a_g$ orbital in the *anti* conformer, the ADC(3) calculations on the *gauche* form indicate a complete breakdown of the orbital picture of ionization for the 3a orbital, with enhanced shake-up splitting due to symmetry lowering. Despite the inclusion of the 3a spectral contribution in the simulation, a discrepancy of 0.6 eV with experiment still remains for the innermost peak, which is essentially due to the fact that at the ADC(3) level 2h-1p shake-up configurations are treated consistently only through first-order in correlation. A shoulder on the high-energy side of this peak is seen in all the experimental (e,2e) spectra, together with less pronounced structures embedded within a long correlation tail at binding energies above 26 eV. These structures and tail relate to a quasi-continuum of shake-up transitions with particularly small intensity (Γ < 0.005).[22b] These were not considered here, since the orbital (MO1 : $3a_g$/3a) from which they borrow nearly exclusively their intensity shows very little sensitivity to conformational alterations (Table 2). Beyond 26 eV, the intensity distribution between the shake-up lines and shake-off bands derived from the $3a_g$ and 3a orbitals will also very certainly match the mole fractions of the *anti* and *gauche* conformers. At this stage, it is worth noting that in straightforward analogy with the simulations reported in ref 22a, the slightly stronger shake-up fragmentation observed for ionization of the *gauche*-3a orbital ***does not*** lead to an additional band broadening compared with the *anti*-$3a_g$ orbital. Quite importantly too, the spectroscopic strengths which

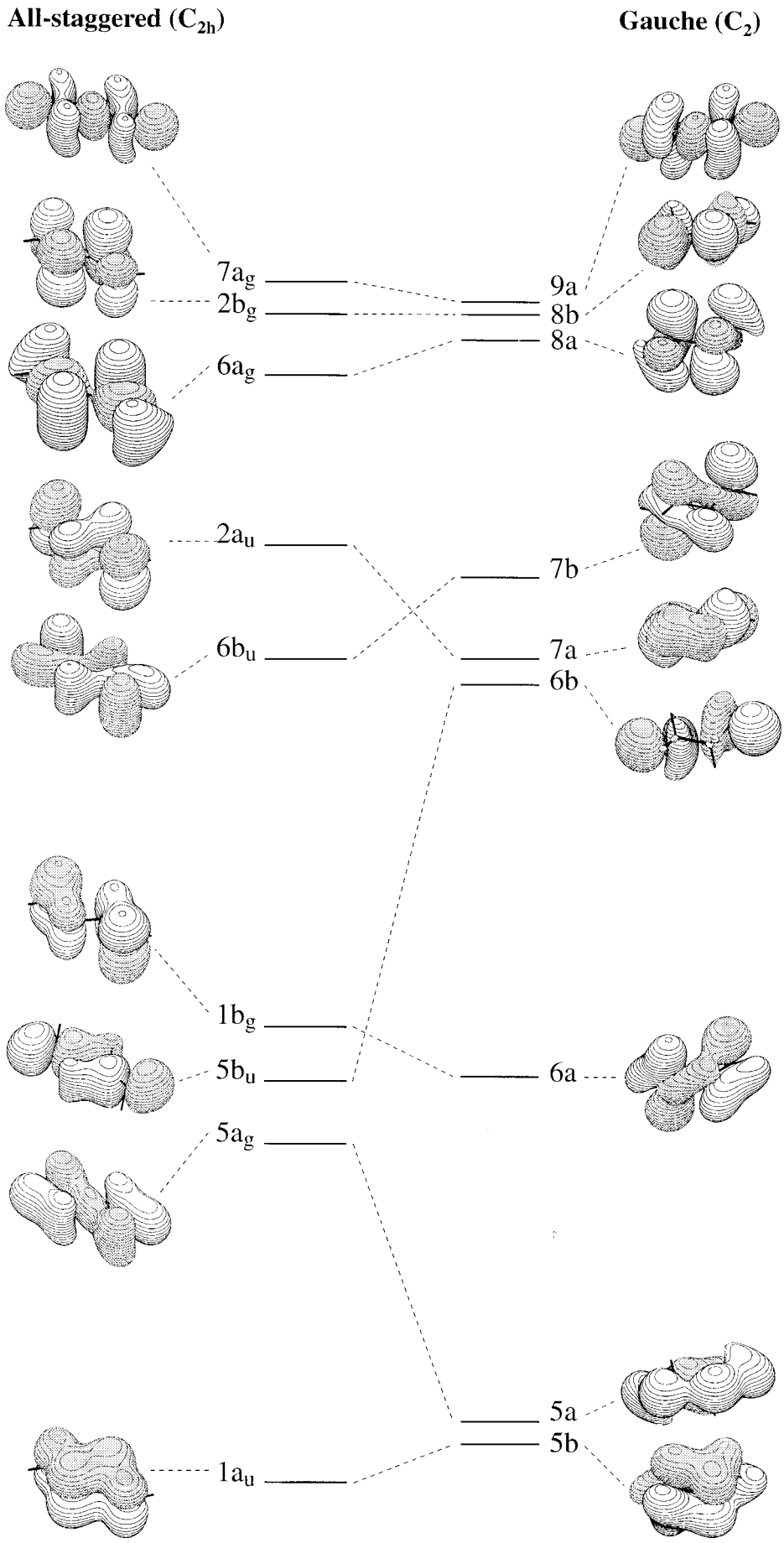

Figure 3. *anti*−*gauche* orbital correlation in the outer-valence region of *n*-butane.

Table 2. Comparison of Various Experimental and Theoretical Results for the Ionization Energies (in eV) of the *all-staggered* (C_{2h}) and *gauche* (C_2) Forms of *n*-Butane.

experimental results						theoretical results (6-311G** basis set)				
valence orbital	EMS ref [24]	XPS ref [13]	HeII ref [15]	HeII ref [16]	HeI ref [14]	HF [C_{2h}]	1p-GF/ADC(3) [C_{2h}]	HF [C_2]	1p-GF/ADC(3) [C_2]	1p-GF/ADC(3) [thermal averaging]
MO1 : $3a_g$, 3a	24.69	24.73	24.63	24.7		29.06	25.41 (0.082)[b] 25.18 (0.160)[b] 25.16 (0.148)[b]	29.04	25.365 (0.106)[b] 25.274 (0.087)[b] 25.159 (0.115)[b] 25.085 (0.085)[b]	25.25[c]
MO2 : $3b_u$, 3b	23.01	23.00	22.99	23.0		26.65	23.51 (0.464)[b] 23.39 (0.141)[b]	26.53	23.543 (0.096)[b] 23.389 (0.574)[b]	23.51[c]
MO3 : $4a_g$, 4a	20.81	20.81	20.74	20.7		23.43	21.06 (0.829)	23.74	21.324 (0.824)	21.14[c]
MO4 : $4b_u$, 4b	19.02	19.11	18.98	18.80	[18.90][a]	21.42	19.44 (0.854)	21.12	19.215 (0.858)	19.40[c]
MO5 : $1a_u$, 5b	15.71		15.72		15.99[a]	17.31	16.19 (0.897)	16.91	*15.818* (0.899)	16.16[d]
MO6 : −, 5a						-	-	16.80	*15.738* (0.900)	*15.80*[d]
MO6 : $5a_g$, −					15.59[a]	15.87	14.90 (0.903)	-	-	
MO7 : $5b_u$, 6a	14.38		14.46		15.50[a]	15.61	14.63 (0.903)	15.59	14.653 (0.906)	14.63[d]
MO8 : $1b_g$, 6b					14.2[a]	15.41	14.52 (0.907)	14.50	*13.670* (0.910)	
MO9 : −, 7a						-	-	14.43	*13.536* (0.908)	*13.58*[d]
MO9 : $6b_u$, −	12.89		12.67		13.2[a]	13.99	13.17 (0.909)	-	-	13.13[d]
MO10 : $2a_u$, 7b					12.74[a]	13.46	12.72 (0.913)	13.69	12.912 (0.911)	12.80[d]
MO11 : $6a_g$, 8a					12.3[a]	12.76	11.95 (0.910)	12.57	11.834 (0.914)	
MO12 : $2b_g$, 8b	11.57		11.36		11.66[a]	12.54	11.83 (0.916)	12.46	11.708 (0.912)	11.78[d]
MO13 : $7a_g$, 9a					11.09[a]	12.42	11.620 (0.909)	12.42	11.644 (0.910)	

[a] Assignment of Kimura et. al.[14] [b] Most dominant lines only ($\Gamma > 0.08$). [c] Through convolution with a FWHM parameter of 1.7 eV and [d] of 0.40 eV. See Appendix I for a detailed discussion of the results by Kimura et. al.[14] Ionization energies labelled with italic character refer to prominent spectral features of the *gauche* [C_2] form of *n*-butane.

through summation are recovered altogether for the $3a_g$ and 3a orbitals are nearly the same, 0.745 and 0.685, respectively, despite the neglect of ionization lines with a pole strength smaller than 0.005 and the amplification of the shake-up fragmentation in the *gauche* form. Nevertheless, it can already be noticed from the simulated (e,2e) spectra that on comparison with the other valence levels, the relative intensities of the lines pertaining both to the *gauche*-3a and to the *anti*-$3a_g$ orbitals are very significantly decreased at the largest azimuthal angles ($\phi = 8$ and 10°), in qualitative agreement with the (e,2e) intensities recorded around 25 eV.

As for the *anti*-$3b_u$ orbital, some shake-up fragmentation is noticed for the 3b orbital of the *gauche* form (Table 2). In this case, the spectroscopic strengths (0.58 versus 0.46) of the most intense line indicates that the orbital picture of ionization is substantially restored compared with the *all-staggered* situation, due to the slight destabilization (by 0.12 eV) of the second orbital in the *gauche* form. This, as well as the destabilization by ∼0.3 eV of the fourth valence orbital, $4a_g$ (4a), leads in the *gauche* form to an ADC(3) result for the ionization energy which is in significantly better agreement with experiment. On the other hand it should be noted that the stabilization by ∼0.3 eV of the third valence orbital in the *gauche* form is apparently at odds with the reported experimental ionization energies.

In the outer-valence region, the large energy variations encountered (Table 2) from MO7 to MO10 with the *anti*-to-*gauche* rotation are at the origin of the considerable modifications observed in the shape of bands. At large azimuthal scattering angles, the outer-valence (e,2e) ionization bands of the *all-staggered* form exhibit two well-distinct peaks near binding energies of 15.5 and 12 eV, which merely encompass the ($5a_g$, $5b_u$, $1b_g$) and ($6a_g$, $2b_g$ and $7a_g$) sets of orbitals, respectively. A minimum in the calculated (e,2e) intensities is then found at about 13.5 eV, as well as a shoulder at ∼16 eV, which fingerprints the $1a_u$ orbital. If the peak simulated at 12 eV matches fairly well the (e,2e) records, very significant disagreement is seen with the position and shape of the other peak at 15.5 eV—by far and large one of the most striking spectral evidences for a deviation from the *all-staggered* form.

Three peaks marginally emerge near 15.8, 13.5, and 12 eV from the outer-valence band of the *gauche* conformer, which are due to the (5b, 5a), (6b, 7a, 7b), and (8a, 8b, 9a) sets of orbitals, respectively. Despite the lower weight of the *gauche* form in the Boltzmann averaging, the presence of the orbital doublet (5b, 5a) at ∼15.8 eV significantly affects the shape, position and width of the peak found at ∼15 eV in the (e,2e) spectrum simulated for the conformer mixture, enabling a much better overall agreement with experiment. More specifically, one can note a striking broadening of this peak as well as a shift of the maximum by ∼1 eV toward lower binding energies. The orbital doublet (6b, 7a) which falls near 13.6 eV also largely compensates for the intensity minimum encountered at ∼13.5 eV in the outer-valence ionization band derived from the *anti* form. At the largest azimuthal scattering angles ($\phi = 8$ and 10°), this minimum is completely concealed by the *gauche* contribution to the thermally averaged (e,2e) spectra, which is perfectly in line with the EMS measurements. Quite clearly, the agreement with the recorded (e,2e) outer-valence bands could be substantially improved by considering a larger proportion of the *gauche* form in the conformer mixture describing *n*-butane.

III. B. Orbital Topologies and Electron Momentum Profiles. Following the recipe already employed for the (e,2e) ionization spectra, the momentum-space orbital densities inferred[25] from the angular dependences of the recorded (e,2e) intensities are compared (Figure 4a−h) to the theoretical profiles of the conformer mixture at room temperature (solid line), as well as with the Boltzmann-weighted individual contributions of the *all-staggered* (dashed line) and *gauche* (dotted line) forms of *n*-butane. Since the (e,2e) spectral resolution of 0.86 eV did not allow for the separation of two overlapping peaks separated by a gap of less than 0.67 eV, we reconsider the partition employed in ref 25 for the deconvolution of the outer-valence band, which was decomposed into four Gaussian contributions with variable width and located at binding energies of 15.71,

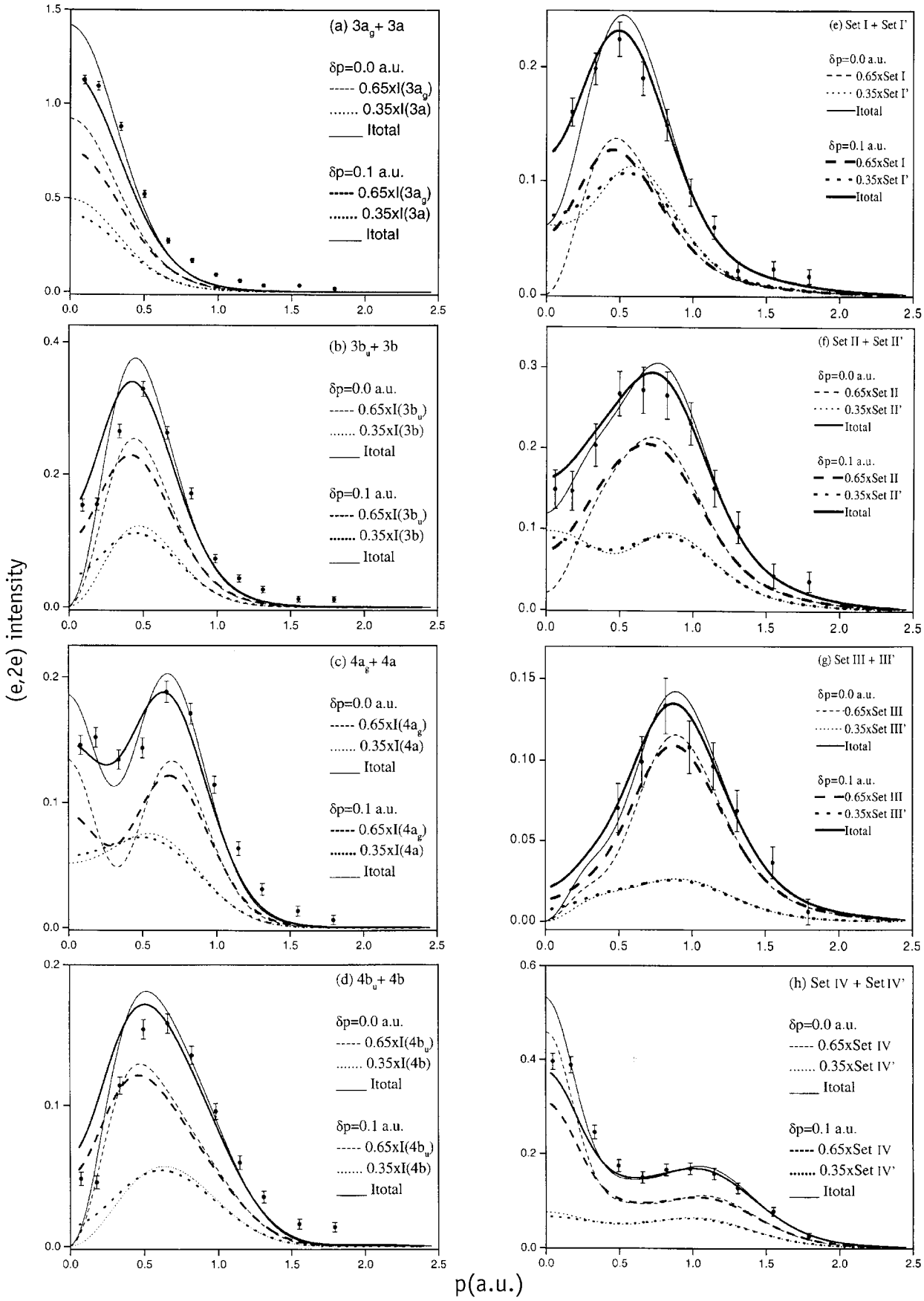

Figure 4. Experimentally resolved and theoretical electron momentum profiles of *n*-butane calculated for an (e,2e) spectrometer with a resolution $\delta p = 0.0$ or 0.1 a.u. on electron momenta. Dashed line: Boltzmann weighted contribution (65%) of the *all-staggered* form; dotted line: Boltzmann weighted contribution (35%) of the *gauche* form; full line: total (e,2e) electron momentum distribution. [Relative spherically averaged (e,2e) cross sections (in arbitrary units) versus electron momentum (in atomic units, a.u.)].

14.38, 12.89, and 11.57 eV. With regard to the ionization energies presented in Table 2 and to the orbital correlations of Figures 2 and 3, these bands can be consistently described by ionization of the I = {$1a_u$}, II = {$5a_g$,$5b_u$,$1b_g$}, III = {$6b_u$,-$2a_u$}, and IV = {$6a_g$,$2b_g$,$7a_g$} sets of orbitals in the *all-staggered* form, and by ionization of the I′ = {5b,5a}, II′ = {6a, 6b,7a}, III′ = {7b}, and IV′ = {8a, 8b, 9a} sets of orbitals in the *gauche* form, respectively. Similarly, the orbital densities measured[25] for the innermost valence level ($3a_g$, alias 3a) include the contribution from the shoulder at ∼26 eV (and deconvoluted as a correlation band of $3a_g$ character in ref 25).

Here also, although at first glance they might not seem as spectacular as the ones seen in the ionization spectra reported in the previous subsection, significant differences in the momentum-space orbital density profiles can be observed in many cases (Figs. 4b-4h) between the *all-staggered* and the *gauche* forms. This confirms our suggestion that, besides providing qualitative information on orbital symmetries or pseudo-symmetries, the angular dependence of the relative intensities in the (e,2e) spectrum which images molecular orbitals also directly fingerprints the molecular conformation of a very floppy and versatile molecule like *n*-butane. To evaluate quantitatively the impact of torsion of the carbon backbone and to establish a connection with the ionization spectra displayed previously, (e,2e) cross sections calculated for a resolution of 0.1 a.u. on electron momenta are illustrated in Figure 5a−h for the outer-valence orbitals.

As for the ionization energies, the electron momentum profiles calculated for the innermost valence orbital show practically no conformational dependence, except for a minor contraction toward $p = 0.0$ a.u., upon torsion from the *all-staggered* to the *gauche* form. Both the momentum-space $3a_g$ and 3a orbitals exhibit a maximum of their one-electron density at $p = 0.0$ a.u., which is typical of an "s-type" symmetric (*gerade*) orbital. The contribution of this orbital therefore dominates in the ionization spectrum recorded at $\phi = 0°$ (Figure 1a), and tends to vanish from the spectra recorded at larger azimuthal angles (see, e.g., Figure 1h).

Conversely, orbitals which correlate with the *ungerade* irreducible representations of the C_{2h} point group can be regarded as being of "p-type", and as such are characterized by (e,2e) cross sections that tend to vanish at $\phi = 0°$ (Figure 1a), that is, for values of p approaching 0.0 a.u. (see, e.g., Figure 4b, 4d, 4e) [these cross sections would truly vanish at $p = 0.0$ a.u. with a resolution parameter of 0.0 a.u. on electron momenta]. The contribution of such orbitals gradually becomes more prominent in the spectra recorded at larger azimuthal angles (Figure 1c−1f), that is, at larger electron momenta. Very generally, in this case, a *spreading* of the orbital densities toward larger electron *momenta* is seen in the simulations (see, e.g., Figure 4b and 4d), when *n*-butane evolves from its *all-staggered* to its *gauche* form. This, undoubtedly, relates to a *contraction* of the related electron densities in *position* space. The *anti*-$3b_u$, $4b_u$, and $1a_u$ orbitals transformed by means of the GW-PG method exhibit a maximum in their orbital density profiles at electron momenta ∼0.42, ∼0.46, and ∼0.45 a.u. whereas the maximum of the *gauche*-3b, 4b, and 5b orbitals is found at electron momenta ∼0.46, ∼0.62, and ∼0.54 a.u., respectively. The effect of torsion is noticeably much stronger for the fourth valence orbital ($4b_u$/4b). This clearly reflects the importance of electron confinement in a position-space orbital with pronounced *anti*-bonding character (in this case: three nodal planes, see Figure 2), which the *anti*-to-*gauche* conversion obviously enhances because of the *out-of-phase* relationship that prevails in this case between the end methyl groups. These shifts of the "p-type" orbital densities toward larger electron momenta in the *gauche* form appear very generally to result in an improved agreement with the cross sections inferred from the (e,2e) measurements. As with the outer-valence (e,2e) ionization bands, increasing the contributions of the *gauche* form in the simulations would clearly yield a better agreement with the electron momentum distributions inferred for the $3b_u$ and $4b_u$ orbitals.

The case of the third valence electron level, $4a_g$ in the all-staggered form, 4a in the *gauche* form, is particularly interesting since qualitative differences in the shape of these orbitals (Figure 2) can be directly recognized in their electron momentum profiles (Figure 4c), and traced experimentally. A mixed "s-p-type" electron momentum distribution with two maxima of electron density at $p = 0.0$ a.u. and 0.67 a.u., and one minimum at 0.30 a.u., was predicted[25] for the momentum-space $3a_g$ orbital. This is consistently supported by the resemblance of the position-space $3a_g$ molecular orbital (Figure 2) with a d_{z^2} atomic orbital, that is, by the presence of two distinct and approximately parallel nodal surfaces. The (e,2e) profile simulated for the $3a_g$ orbital is qualitatively in agreement with the recorded (e,2e) cross sections, although the depletion of the intensity at electron momenta around 0.3 a.u. is much too pronounced. This defect is superbly corrected when the contribution of the *gauche*-4a orbital is incorporated in the simulation (Figure 4c). In momentum space, in sharp contrast with the $3a_g$ orbital, the 3a orbital only displays one maximum of its electron density at $p = 0.50$ a.u., and one minimum at $p = 0.0$ a.u., and can therefore be regarded as approaching a "p-type" profile. This striking variation in the qualitative appearance of the momentum distributions relates to the fact that one of the two nodal planes present in the *anti*-$3a_g$ orbital has effectively been released by the conversion into the *gauche*-3a orbital. As a matter of fact, the latter closely resembles in shape the $3a_1$ orbital of the water molecule, which is also characterized by a "p-type" electron momentum profile (see Figure 3c of ref 41 for a comparison). Besides these changes of shape, the shift upon torsion of the orbital densities toward lower electron momenta is due in this case to through-space bonding interactions between the end-methyl groups in the *gauche* form, which obviously help to limit the importance of electron confinement in position space.

The theoretical results displayed in Figure 5a for the $5a_g$ orbital indicate major alterations of its electron momentum profile upon the *anti*-to-*gauche* conversion of *n*-butane, which corroborates a stabilization by 0.8 eV in the *gauche* form. Here also, the transformation of an orbital with two nodal planes across the carbon backbone into an orbital with only one nodal surface and strongly enhanced bonding character is noted (Figure 3) when *n*-butane evolves from its *all-staggered* into its *gauche* forms. This is at the origin of a very striking transfer of the electron densities toward the lower momenta, as can be seen when comparing the EMS profiles of the 5a and $5a_g$ orbitals. Conversely, and this time in line with a destabilization by 0.96 eV, a substantial transfer toward the most remote regions of momentum-space is seen upon torsion for the $5b_u$ orbital (Figure 5b), owing to the disruption of bonding interactions around the central C−C bond and thereby the creation of one additional nodal surface (Figure 3) in the 6b orbital. Only a slight expansion of the momentum profile is seen for the conversion of the $1b_g$ orbital into the 6a one (Figure 5c), which in this case corroborates a minor stabilization by 0.13 eV. Torsion of the $6b_u$ orbital into the 7b one, which both exhibit three nodal surfaces accross the carbon backbone (Figure 3), induces some broadening in the related orbital density (Figure 5d). The

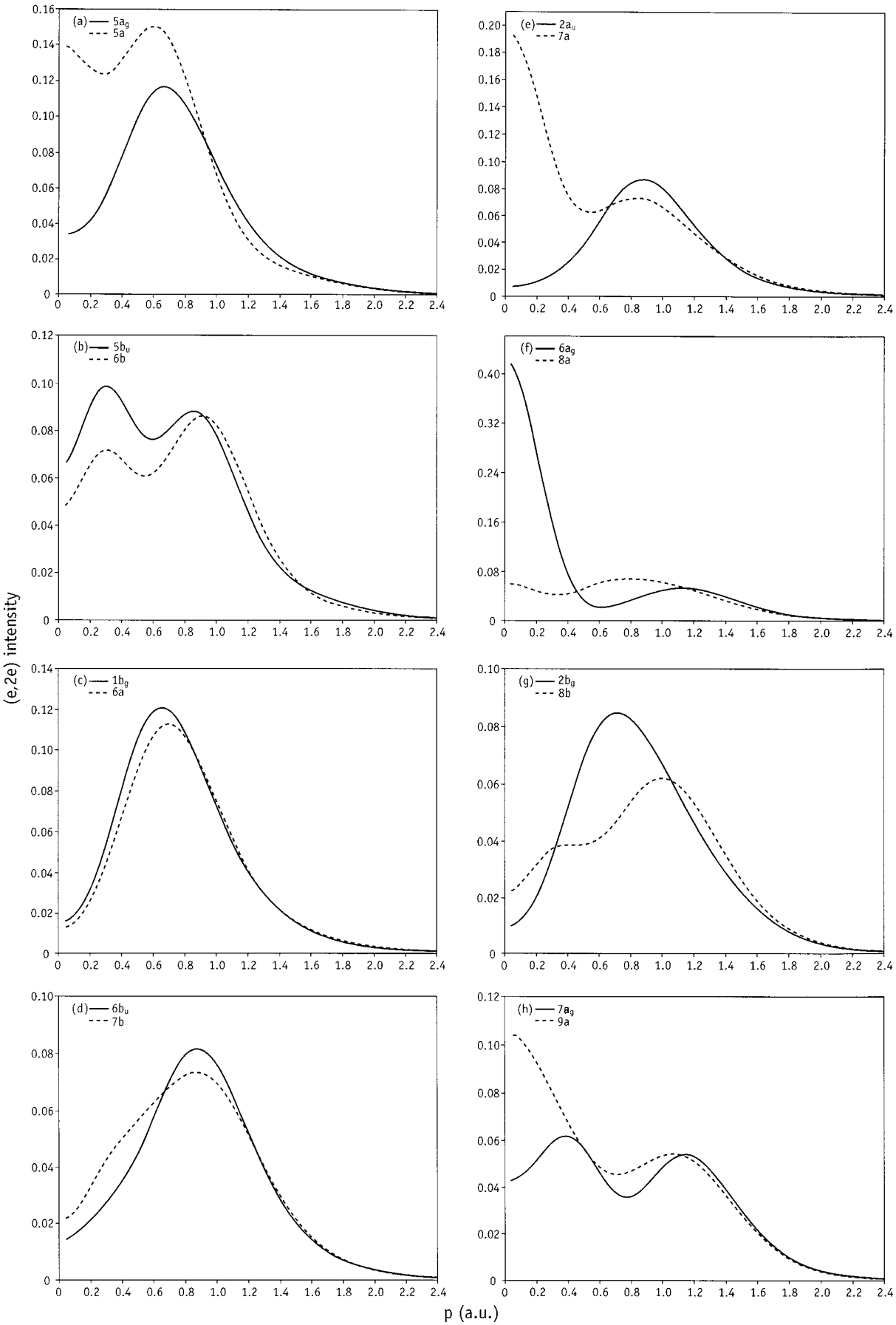

Figure 5. Detailed comparison of the outer-valence momentum-space orbital densities of *n*-butane. [Relative spherically averaged (e,2e) cross sections (in arbitrary units) versus electron momentum (in atomic units, a.u.)]. Results pertain to an experimental resolution δp of 0.1 a.u. on momenta.

stabilization by 0.97 eV due to the conversion of the $2a_u$ orbital into the 7a one is unsurprisingly fingerprinted by a very significant increase of the (e,2e) cross section at low electron momenta (Figure 5e). This time, an EMS profile with only one extremum at $p = 0.88$ au is transformed into an intensity curve characterized by a rather sharp maximum at $p = 0.00$ a.u., and another looser maximum at $p = 0.83$ a.u. With regard to our previous observations for the third inner-valence orbital ($4a_g$, 4a), these variations are explained consistently by the obliteration of the nodal surface along the *all-staggered* carbon backbone in the $2a_u$ orbital, leaving two approximately parallel nodal surfaces across the *gauche* backbone in the 7a orbital.

Owing to the strong impact of the *anti*-to-*gauche* torsion on one-electron binding energies, to the rather arbitrary character of our orbital partition, and to the limited resolution (1.7 eV) of the (e,2e) spectrometer, the electron momentum distributions pertaining to the orbitals of sets I−I′, II−II′, and III−III′ must be compared with extreme caution with the deconvoluted outer-valence (e,2e) cross sections (Figure 4e−g). The most striking outcome of these variations is that orbital set II displays overall a "p-type" profile, characterized by only one maximum at $p = 0.7$ eV, whereas set II′ shows a mixed "s-p-type" character, with an additional maximum at $p = 0.0$ a.u., due merely to orbital 7a, respectively. For these orbital sets, the *gauche* form of *n*-butane tends therefore to compensate the limitation of the orbital density at the lowest electron momenta, which seems to be in line with the (e,2e) cross sections (Figure 4f) deconvoluted from the middle of the outer-valence region, that is, near binding energies of 14.4 eV. The analysis (Figure 4e) of the (e,2e) records at binding energies near 15.7 eV is also slightly complicated by the contribution of orbital 5a, which tends to substantially limit the depletion of the (e,2e) cross sections near $p = 0.0$ a.u. Despite this orbital, the overall profile of sets I + I′ still markedly reflect the dominant "p-type" character of orbitals $1a_u$ and 5b, and still remain in very fair agreement with the (e,2e) measurements. At last, the (e,2e) cross sections that arise from the *gauche* conformer at binding energies near 12.9 eV (Figure 4g) reduce to the sole contribution of orbital 7b. This explains a rather significant limitation of the (e,2e) intensities at $p \sim 1.0$ a.u., which tends also to slightly improve the agreement with the measurements.

In the outer-valence region, the most striking and indubitable evidence given by the electron momentum distributions for a deviation from the *all-staggered* form is found with the correlation between the $6a_g$ and 8a orbitals, which contribute very differently (Figure 5f) to the EMS profiles of sets IV and IV′ (Figure 4h), respectively. The $6a_g$ orbital has a very peculiar topology (Figure 3), with only one closed nodal surface which resembles a "highly stretched and nearly dividing prolate ellipsoid". In this orbital, the most prominent contributions arise from the C−H bonds, which therefore implies electron delocalization at large distances with respect to the molecular center of mass. Rather unsurprisingly therefore, this orbital yields a particularly sharp and intense rise of the (e,2e) cross sections at vanishing electron momenta (Figure 5f). The related electron momentum distribution is also characterized by one minimum at $p = 0.62$ a.u., as well as another loose maximum at $p = 1.14$ a.u. Besides reducing nonbonded interatomic distances, the conversion upon torsion of this orbital into its *gauche*-8a counterpart leads to a much more intricate nodal pattern. In momentum space, the final outcome of this transformation is a major decrease of the orbital density near $p = 0.0$ a.u., a shift of the second extremum from $p = 1.14$ a.u. to $p = 0.80$ a.u., and altogether a very significant broadening of the EMS profile. These variations are very partially compensated for by the splitting (Figure 5g) of the "p-type" electron momentum distribution arising from orbital $2b_g$, with one maximum at $p = 0.74$ a.u., into two peaks at $p = 0.4$ a.u. and $p = 1.00$ a.u., which emphasizes again the obliteration of a nodal plane along the *all-staggered* carbon backbone. Another compensation is due to a significant increase of the electron momentum density at the lowest electron momenta with the conversion of the *anti*-$7a_g$ orbital into the *gauche*-9a orbital (Figure 5h), which enlightens the *in-phase* orbital relationships that prevail in this case between the end-methyl groups. Owing to the major effect of the torsion of *n*-butane on the EMS profile fingerprinting the $6a_g$ orbital, accounting for the *gauche* conformer by means of thermal averaging at 298K considerably improves the agreement with the (e,2e) cross sections inferred below $p = 0.5$ a.u. by deconvolution of the band at ~11.6 eV (Figure 4h).

Concluding Remarks

A first analysis[25] of the electron momentum spectra recorded on *n*-butane has been improved by considering explicitly the effect of thermal motions in the gas phase, by means of a Boltzmann averaging of the conformer populations at room temperature. Besides confirming the intimate relation of the angular dependence of the ionization cross sections to orbital symmetries or pseudo-symmetries, this study demonstrates very convincingly the current and largely unexploited potential of electron momentum spectroscopy as a conformational probe. To enable a safe identification of the spectral features fingerprinting a given molecular conformation, EMS measurements have been compared with the results of large-scale ADC(3) one-particle Green's Function calculations of ionization spectra together with the transformation to momentum-space of Kohn−Sham DFT(B3LYP) orbitals, a combination which ensures a thorough treatment of both static (initial-state) and dynamic (final-state) electronic correlation. The use of Hartree−Fock orbitals in the one-particle Green's Function ADC(3) computations, and of Kohn−Sham orbitals in the calculation of electron momentum densities, may make this up to now very successful and commonly employed procedure (see, e.g., refs 24, 26−30) somewhat inconsistent. A possible way to cure this inconsistency would be to replace the Kohn−Sham orbitals by Dyson orbitals[42] directly obtained from the Green's Function ADC(3) calculations.

Simulations based upon these theoretical grounds have shown that both one-electron binding energies and orbital densities in momentum-space very sensitively reflect the topological alterations that the molecular orbitals undergo when *n*-butane evolves from its *all-staggered* to its *gauche* forms. Most generally, torsion stabilizes orbitals which display an even number of nodal surfaces *across* the carbon backbone in the *all-staggered* form, and conversely destabilizes those with an odd number of planes. Contraction or expansion of orbital densities correspondingly occur in momentum-space, which sensitively reflect a release or enhancement of electron confinement in position-space. In a few cases ($4a_g$, $5a_g$, $2a_u$, $6a_g$), due to symmetry-lowering, torsion also implies the obliteration or creation of one nodal plane in the molecular orbital, which in turn leads to very recognizable variations in the qualitative appearance of the related electron momentum profiles. Even when ionization lines are not completely resolved, "composite" ionization bands still exhibit very characteristic clues of the presence of the *gauche* conformer, both in terms of their shape, binding energies, and of the angular dependence of their (e,2e) cross sections.

Quite clearly, from a global comparison of our simulations with the recorded (e,2e) ionization spectra as well as with the

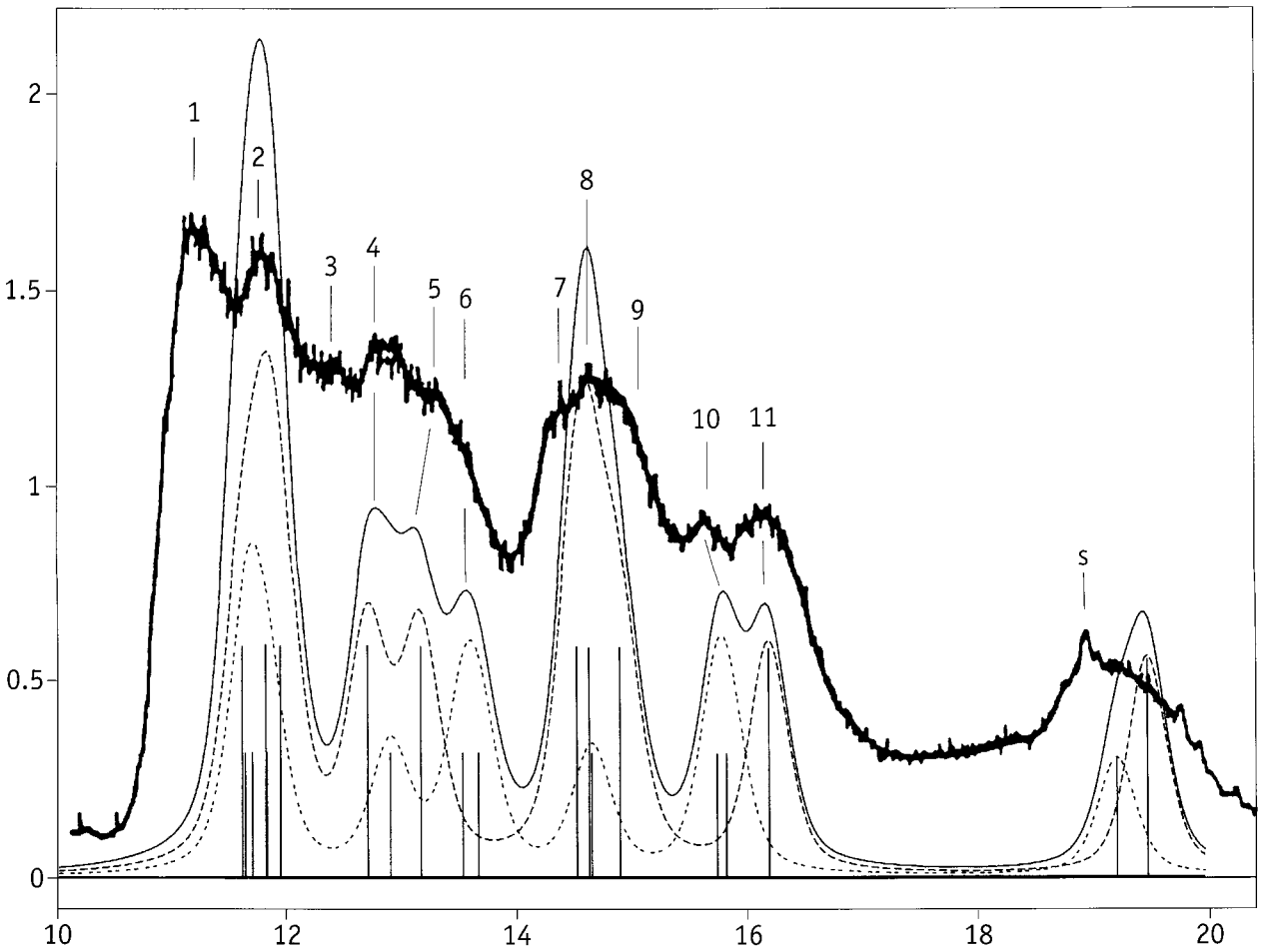

Figure 6. 1p-GF/6-311G** analysis of the HeI ionization spectrum recorded on *n*-butane by Kimura et al.[14] [FWHM = 0.4 eV]. Dashed line: Boltzmann weighted contribution (65%) of the *all-staggered* form; dotted line: Boltzmann weighted contribution (35%) of the *gauche* form; full line: total ionization spectrum. [Boltzmann weighted spectral intensities and convoluted densities of states versus electron binding energies (in eV)].

inferred orbital density profiles, the agreement with experiment could certainly be improved markedly overall by considering a larger proportion of the *gauche* form in the conformer mixture. This would imply either a higher temperature or a substantially reduced *anti-gauche* free energy difference. At this stage, it is worth recalling that the (e,2e) measurements[23,25] reinvestigated in this work were recorded on gas-phase samples injected directly, that is, at room temperature, in the high-vacuum [$5 \cdot 10^{-7}$ Torr] chamber of the (e,2e) spectrometer, but—quite unfortunately—without any specific temperature measurements in this chamber, following the most common practices in this field as well as in photoionization spectroscopy. However, the pressure differences between the butane container and the vacuum chamber, which speeds up the molecules into supersonic jets, as well as the considerable energies that are coming into play with the (e,2e) ionization processes may on the time scale of the experiment lead to considerable variations of the temperature within the interaction region where these processes occur. A main conclusion of this theoretical investigation is thus to advocate better and systematic control of this important experimental parameter in (e,2e) or photoelectron measurements of all kind, despite the considerable difficulties that this may imply: very often, the interaction region is subject to considerable energy transfers and pressure differences, and presumably therefore to the laws of non linear thermodynamics.

Further combined theoretical and experimental studies on larger saturated hydrocarbons (*n*-pentane, *n*-hexane, ...) should clearly be carried out to confirm in more challenging situations the potential of electron momentum spectroscopy as a conformational probe. In the long term, the effect of thermal motions on the (e,2e) or ionization spectra of such versatile species could also be described in a more consistent way, in order to account for the transitions between the local energy minima. One should in particular couple the computation of such spectra with molecular dynamics simulations or Monte Carlo sampling.

Acknowledgment. M.S.D. and A.S. acknowledge financial support from the "Bijzonder Onderzoeksfonds" (BOF) of the Limburgs Universitair Centrum (LUC, Belgium), and from the "Fonds voor Wetenschappelijk Onderzoek van Vlaanderen", the Flemish Science Foundation. They are grateful to Professor J.-P. François (LUC) for useful discussions, support, and encouragements. W.P. is grateful to the National Science Foundation of China (NSFC) for a Grant under Contract No. 19874037.

Appendix: The He(I) UPS Spectrum by Kimura *et al.*[14]

Lacking better tools, the high-resolution He(I) spectrum taken on *n*-butane in 1981 by Kimura et al [14] was first interpreted as reported in Table 2 by means of HF/4-31G calculations. Although the presence of the *gauche* conformer was correctly suspected because of the presence of a peak at ~15.5 eV, the neglect of electronic correlation and relaxation has led to erroneous assignments of some ionization bands. To safely reassign this spectrum, we display in Figure 6 the result of a

convolution of our 1p-GF/ADC(3) results using as a broadening function a combination of one Gaussian and one Lorentzian with equal weight, a FWHM parameter of 0.4 eV, and an intensity scaled according to the computed spectroscopic strengths Γ. Here also, a mole fraction of 0.35 has been considered for the *gauche* conformer. From a comparison of the final outcome of our simulation with the measurement by Kimura et al., it is clear that the shoulder at 13.6 eV and the peak at 15.5 eV fingerprint orbitals of the *gauche* form, namely the {6b,7a} and the {5b,5a} orbital doublets, respectively (see Table 2 for details). A rather obvious discrepancy can be seen between our simulation based on high-order *vertical* ionization energies and the high-resolution He(I) measurements by Kimura et al.[14] The former displays a sharp and intense peak at the ionization threshold (11.8 eV), whereas on the experimental side the contribution of the three outermost orbitals is clearly recovered within two or possibly three peaks (with labels 1−3 in Figure 6) with approximately equal and lower intensity at 11.09, 11.66 and 12.3 eV (Table 2). With regard to the expected accuracy (∼0.2 eV) of the ADC(3)/6-311G** calculations,[25] this discrepancy can at first glance only be explained by a substantial deviation from a vertical ionization process, in the form of vibronic interactions between different ionized states. The latter are indeed very likely to occur due to the large conformational freedom and the near energy degeneracy (within 0.3 eV) of the three outermost orbitals of *n*-butane.

The following assignment is therefore proposed:

peaks 1-3 (11.09, 11.66, 12.3 eV):	IV=$\{6a_g,2b_g, 6a_g\}$ + IV′={8a, 8b, 9a}
peak 4 (12.74 eV):	$2a_u$ [C_{2h}]
peak 5 (13.2 eV):	$6b_u$ [C_{2h}]
shoulder 6 (13.5 eV):	{7a,6b} [C_2]
peaks 7-9 (14.2, 14.52, 15.0 eV):	II=$\{1b_g, 5b_u, 5a_g\}$ + 6a [C_2]
peak 10 (∼14.5 eV):	[5a, 5b} [C_2]
peak 11 (15.99 eV):	$1a_u$ [C_{2h}]

JA0039886